Analytical and numerical analysis of bifurcations in thermal convection of viscoelastic fluids saturating a porous square box

A. Taleb, H. BenHamed, M. N. Ouarzazi, and H. Beji

Citation: Physics of Fluids **28**, 053106 (2016); doi: 10.1063/1.4948532
View online: http://dx.doi.org/10.1063/1.4948532
View Table of Contents: http://scitation.aip.org/content/aip/journal/pof2/28/5?ver=pdfcov
Published by the AIP Publishing

PHYSICS OF FLUIDS **28**, 053106 (2016)

Analytical and numerical analysis of bifurcations in thermal convection of viscoelastic fluids saturating a porous square box

A. Taleb,[1] H. BenHamed,[2,a)] M. N. Ouarzazi,[3] and H. Beji[2]
[1]*Laboratory of dynamics and vibro-acoustic engines, National Institute of Engineering Mechanics, University of Boumerdes, Boumerdes, Algeria*
[2]*Laboratoire des Technologies Innovantes, EA 3899, Université de Picardie Jules Verne, Avenue des Facultés, 80025 Amiens, France*
[3]*Laboratoire de Mécanique de Lille, UMR CNRS 8107, Université de Lille I, Bd Paul Langevin, 59655 Villeneuve d'Asq, France*

(Received 25 June 2015; accepted 11 April 2016; published online 23 May 2016)

We report theoretical and numerical results on bifurcations in thermal instability for a viscoelastic fluid saturating a porous square cavity heated from below. The modified Darcy law based on the Oldroyd-B model was used for modeling the momentum equation. In addition to Rayleigh number $\mathfrak{R}$, two more dimensionless parameters are introduced, namely, the relaxation time λ_1 and the retardation time λ_2. Temporal stability analysis showed that the first bifurcation from the conductive state may be either oscillatory for sufficiently elastic fluids or stationary for weakly elastic fluids. The dynamics associated with the nonlinear interaction between the two kinds of instabilities is first analyzed in the framework of a weakly nonlinear theory. For sufficiently elastic fluids, analytical expressions of the nonlinear threshold above which a second hysteretic bifurcation from oscillatory to stationary convective pattern are derived and found to agree with two-dimensional numerical simulations of the full equations. Computations performed with high Rayleigh number indicated that the system exhibits a third transition from steady single-cell convection to oscillatory multi-cellular flows. Moreover, we found that an intermittent oscillation regime may exist with steady state before the emergence of the secondary Hopf bifurcation. For weakly elastic fluids, we determined a second critical value $\mathfrak{R}_2^{Osc}(\lambda_1,\ \lambda_2)$ above which a Hopf bifurcation from steady convective pattern to oscillatory convection occurs. The well known limit of $\mathfrak{R}_2^{Osc}(\lambda_1 = 0,\ \lambda_2 = 0) = 390$ for Newtonian fluids is recovered, while the fluid elasticity is found to delay the onset of the Hopf bifurcation. The major new findings were presented in the form of bifurcation diagrams as functions of viscoelastic parameters for $\mathfrak{R}$ up to 420. *Published by AIP Publishing.* [http://dx.doi.org/10.1063/1.4948532]

I. INTRODUCTION

The knowledge and the control of the behavior of instabilities in non-Newtonian fluids are of interest in many fields of science and engineering. In particular, viscoelastic fluids can be found in a great number of applications such as those in bio-engineering and in pharmaceutical and petroleum industries, among others. Most of the existing studies dealing with viscoelastic fluids focus either on hydrodynamic instabilities under isothermal conditions[1] or on thermal instabilities.[2–10] In the latter case, linear stability analysis reveals that the onset of natural convection of viscoelastic fluids can be oscillatory instead of stationary, depending on the fluid elasticity. This behavior was confirmed by the experimental results[7] of Kolodner using DNA suspensions. Without DNA suspensions, no oscillations on any time scale were observed in these control experiments. In the presence of DNA

a)Author to whom correspondence should be addressed. Electronic mail: haykel.benhamed@u-picardie.fr

suspensions, experiments reveal that the first convective instability is oscillatory. Even though the buoyancy-driven instabilities in viscoelastic fluids have been extensively studied for clear fluid media, the same cannot be said about their counterparts in the presence of a porous matrix. This is probably due to the crucial problem of the formulation of the constitutive equations regarding viscoelastic fluid flows in porous media.

Recently, some activities[11–15] have been devoted to investigate the primary convection patterns of a viscoelastic fluid confined in a porous medium heated from below by using the modified Darcy's law based on the Oldroyd-B model. Kim *et al.*[11] and Yoon *et al.*[12] performed a linear stability analysis and showed that in viscoelastic fluids such as polymeric liquids, a Hopf bifurcation as well as a stationary bifurcation may occur depending on the magnitude of the viscoelastic parameter. The three-dimensional convective and absolute instabilities of a viscoelastic fluid in the presence of a horizontal pressure gradient have been analyzed by Hirata and Ouarzazi.[13] From the nonlinear point of view, Kim *et al.*[11] carried out a nonlinear stability analysis by assuming a densely packed porous layer and found that both stationary and Hopf bifurcations are supercritical relative to the critical heating rate. The work of Kim *et al.*[11] has itself been extended by Zhang *et al.*[14] to include the effects of the porous parameter Da (Darcy number) which bridges the gap between nonporous cases ($Da \to \infty$) and densely packed porous cases ($Da \to 0$). In the former case, they found that the bifurcation to oscillatory convection can be subcritical. In Ref. 14, the authors focused only on the temporal evolution of standing waves at the onset of oscillatory instability. With infinite horizontal porous cavity, traveling waves are also possible. The question of whether standing or traveling waves are preferred at onset has been fully addressed by Hirata *et al.*[15] In addition to its theoretical interest, Delenda *et al.*[16] have shown that viscoelastic convection in porous media may be useful for industrial applications interested by the separation of species of viscoelastic solutions. The introduction of a porous packing allows to control the average vertical convective velocity (which is a function of the permeability of the medium) and to generate a homogeneous convection current, improving the separation of species.

To our knowledge, the problem of convection of viscoelastic fluids in porous media has been the subject of few numerical investigations.[17–20] Fu *et al.*[17] performed direct numerical simulations on two-dimensional thermal convection of a viscoelastic fluid saturating a porous square cavity. These simulations were conducted for Darcy-Rayleigh number up to 400 and for selected three set values of dimensionless relaxation time λ_1 and dimensionless retardation time λ_2: (i) $\lambda_1 = 0.3$ and $\lambda_2 = 0.2$, (ii) $\lambda_1 = 0.2$ and $\lambda_2 = 0.1$, and (iii) $\lambda_1 = 0.3$ and $\lambda_2 = 0.1$. In order to define clearly the objective of the current study, we reproduced the main results for the three set values of viscoelastic parameters used in Ref. 17. These results are depicted in Fig. 1 which illustrates the asymptotic behaviour of the average Nusselt number Nu as a function of Darcy-Rayleigh number $\mathfrak{R}$. The Newtonian fluid case is also displayed for comparison purposes. The curves shown in Fig. 1 coincide

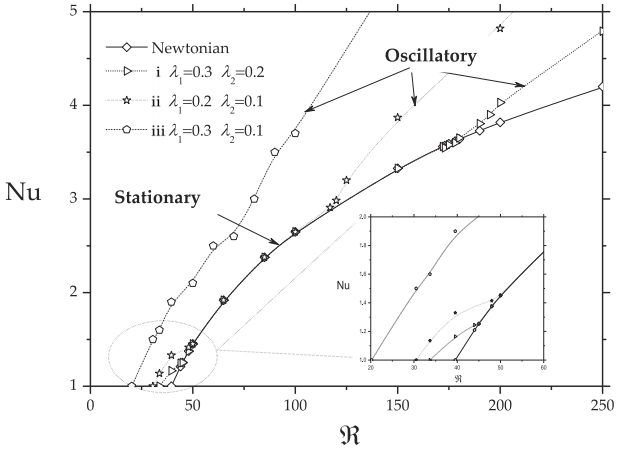

FIG. 1. Nusselt number Nu versus Darcy-Rayleigh number $\mathfrak{R}$ for values of viscoelastic parameters used in Ref. 17, including the Newtonian fluid case.

perfectly with those obtained in Fig. 4 of Ref. 17. As in Ref. 17, we found that when the conduction state loses its stability, the flow oscillates periodically for all three cases, which results in the Nu being oscillatory with time. Furthermore, as can be seen from the inset of Fig. 1, the Nu curve for case (iii) is completely above that for a Newtonian fluid, while part of the Nu curves for the two other cases merge with that for a Newtonian fluid. This last behavior of Nu means that in the nonlinear regime, oscillatory convection for cases (i) and (ii) is completely suppressed and replaced by stationary convection if $\mathfrak{R}$ exceeds a critical value. Furthermore, Fig. 1 also shows that for sufficiently high values of Darcy-Rayleigh number, a clear deviation of the average Nusselt number from a Newtonian behaviour is observed for cases (i) and (ii). Numerical simulations performed in Ref. 17 showed that this qualitative change in Nusselt number is associated with a third transition from stationary convection to oscillatory one. Therefore, a question is raised according to the numerical results of Ref. 17: why these numerical experiments revealed the existence of a second transition from oscillatory convection to stationary one followed by a third transition to oscillatory convection for cases (i) and (ii) while these successive transitions never occur for case (iii)?

The objective of this study is to provide some answers to the above question. More precisely, our aim is to give a global picture in the $(\mathfrak{R}, \lambda_1, \lambda_2)$ space on possible successive bifurcations of convection patterns in a square porous cavity saturated by a viscoelastic fluid. Both theoretical and numerical approaches are used. We first perform a linear stability analysis in order to locate a codimension-two bifurcation point where steady and oscillatory instabilities may develop simultaneously. As a second step, a weakly nonlinear stability approach is proposed to reduce the original complicated problem into a simple model retaining only the most essential features. This method turns out to be very successful to predict the nonlinear dynamics near the codimension-two bifurcation point. In particular, an analytical relation that governs the nonlinear threshold Darcy–Rayleigh number for a secondary bifurcation from oscillatory to steady convection is derived as a function of viscoelastic parameters λ_1 and λ_2. Finally, direct numerical simulations on two-dimensional thermal convection of a viscoelastic fluid saturating a square porous cavity based on the modified Darcy's law are performed. The objective of the numerical simulations is twofold. We first compare numerical results with linear and weakly nonlinear theories. Especially, we determine the extension in the viscoelastic parameters space where the second bifurcation from oscillatory to stationary convection is observed. Second, for high values of Rayleigh number where weakly nonlinear analysis ceases to be valid, numerical simulations identify a third transition from stationary convection to a new oscillatory mode of instability. A general diagram of stability, which provides all the possible bifurcations and convective structures, is determined.

II. THE SYSTEM

A. Problem formulation

We consider a square box filled with a Boussinesq viscoelastic liquid saturating a porous square cavity. Horizontal boundaries are assumed perfectly heat conducting and subjected to constant temperatures; T_0^d on the bottom and T_1^d on the top, with $T_1^d < T_0^d$. The vertical walls are considered impermeable and adiabatic.

The equilibrium between the filtration velocity and the pressure gradient is instantaneous in Newtonian flows. However, for viscoelastic fluids, the equilibrium can only be reached after a certain time. This characteristic time is called relaxation time λ_1^d. Also, the material forgets its initial form after unloading some of its elastic energy into kinetic energy at a second characteristic time called the retardation time λ_2^d with $\lambda_2^d \leq \lambda_1^d$. Typical liquids having viscoelastic behavior are solutions composed of a Newtonian solvent and polymeric solute. Thus, we define the non-dimensional ratio Γ as

$$\Gamma = \frac{\lambda_2}{\lambda_1} = \frac{\lambda_2^d}{\lambda_1^d} = \frac{\mu_s}{\mu_s + \mu_p} = \frac{\mu_s}{\mu}, \tag{1}$$

where μ_s, μ_p, and μ are, respectively, the solvent, the polymer, and the solution viscosities; it is clear that $0 \leq \Gamma \leq 1$. The limit $\Gamma = 0$ recovers a purely elastic fluid or the so-called Maxwell fluid,

and the limit $\Gamma = 1$ corresponds to a much diluted polymer solution (Newtonian behavior). Several approaches exist for modeling the rheological behavior of viscoelastic fluids. The Oldroyd-B *model* is one of the most frequently present in the literature. The viscoelastic stress tensor τ in this model obeys the following system:

$$\begin{cases} \tau_G = -P^d I + \tau, & (2a) \\ \left(1 + \lambda_1^d D_t\right) \tau = \mu \left(1 + \lambda_2^d D_t\right) \gamma, & (2b) \\ D_t \tau = \partial_t \tau + \left(\vec{U}^d . \vec{\nabla}\right) \tau - \left(\vec{\nabla} \vec{U}^d\right)^T \tau - \tau \left(\vec{\nabla} \vec{U}^d\right), & (2c) \end{cases}$$

where τ_G is the global extra-stress tensor, P^d is the pressure, I is the identity tensor, τ is the extra-stress tensor, γ is the deformation tensor, $\vec{U}^d$ is the fluid velocity, and D_t is the Oldroyd derivative. By analogy with Oldroyd-B model, a phenomenological modified Darcy law was given by Alishayev and Mirzadzhanzadeh,[21]

$$\left(1 + \lambda_1^d \partial_t\right) \vec{V}_f^d = -K \mu^{-1} \left(1 + \lambda_2^d \partial_t\right) \left\{\vec{\nabla} p^d + \rho \vec{g} \cdot \vec{e}_z\right\}. \quad (3)$$

$\vec{V}_f^d$ is the filtration velocity defined by the Dupuit's equation: $\vec{V}_f^d = \varepsilon \vec{U}^d$, where ε is the porosity, μ is the dynamic viscosity, K is the permeability, ρ is the fluid density, $\vec{g}$ is the gravitational acceleration, while ∂_t is the partial derivative with respect to time. We adopt the Boussinesq approximation and consider that the density ρ is a linear function of temperature,

$$\rho = \rho_0 \left(1 - \beta \left(T^d - T_1^d\right)\right), \quad (4)$$

where T^d is the temperature field, ρ_0 is the fluid density at the reference temperature T_1^d, and β is the thermal expansion coefficient.

In this study, we consider the local thermal equilibrium between the fluid and the porous matrix. According to the Darcy-Oldroyd-B model, subject to the Oberbeck-Boussinesq approximation, the incompressibility condition, the momentum, and the energy balance equations are given by the following system:

$$\begin{cases} \vec{\nabla} \cdot \vec{V}_f^d = 0, & (5a) \\ \left(1 + \lambda_1^d \partial_t\right) \vec{V}_f^d = -\dfrac{k}{\mu} \left(1 + \lambda_2^d \partial_t\right) \left\{\vec{\nabla} P^d + \rho \left[\beta \left(T^d - T_0^d\right)\right] \vec{g} \cdot \vec{e}_z\right\}, & (5b) \\ \left(\sigma \partial_t + u^d \partial_x + w^d \partial_z\right) T^d = \kappa \left(\partial_x^2 + \partial_z^2\right) T^d, & (5c) \\ T^d(x, 0) = T_0^d, \qquad T^d(x, \mathrm{H}) = T_1^d, \ \partial_x T^d(0, z) = \partial_x T^d(\mathrm{H}, \mathrm{z}) = 0, \qquad \vec{V}_f^d \cdot \vec{n} = 0, & (5d) \end{cases}$$

with κ and σ are, respectively, the effective thermal diffusivity and the volumetric heat capacity ratio between solid and liquid phases.

B. The normalized system

We transform the equations of motion to the dimensionless form using the following reference scales: H for lengths, $\sigma H^2 \kappa^{-1}$ for time, $\Delta T = T_0^d - T_1^d$ for temperature, and κH^{-1} for velocities.

Using the double curl procedure to drop the pressure and the stream function formulation $\psi = \int u dz = -\int w dx$ to express incompressibility, the final normalized system is written as

$$\begin{cases} \partial_t T = \left(\partial_x^2 + \partial_z^2 - u \partial_x - w \partial_z\right) T, & (6a) \\ \left(1 + \lambda_1 \partial_t\right) \mathcal{H} = \Re \left(1 + \lambda_2 \partial_t\right) \partial_x T, & (6b) \\ \left(\partial_x^2 + \partial_z^2\right) \psi = \mathcal{H}, & (6c) \\ T(x, 0) = 1, \quad T(x, 1) = \partial_x T(0, z) = \partial_x T(1, z) = 0, & (6d) \\ \psi(x, z) = 0 \text{ for all boundaries}, & (6e) \end{cases}$$

where $\Re = g \beta \Delta T \mathrm{KH} / (\nu \kappa)$ is the Darcy-Rayleigh number, and $\mathcal{H}$ is the harmonic function of ψ. Equations (6d) and (6e) state, respectively, that horizontal walls are subjected to imposed temperatures and the vertical walls are adiabatic and that the borders of the square box are impermeable.

The limit $\lambda_2 = 0$ recovers a purely elastic fluid or the so-called Maxwell fluid, and in the limit $\lambda_1 = \lambda_2$, the Oldroyd-B fluids tend to Newtonian fluids, which can also be seen from Eq. (6b). Indeed, this equation may be written for $\lambda_1 = \lambda_2$ as

$$\lambda_1 \partial_t (\mathcal{H} - \Re \partial_x T) = -(\mathcal{H} - \Re \partial_x T). \tag{7}$$

The solution to this equation is $\mathcal{H} - \Re \partial_x T \approx e^{-t/\lambda_1}$.

This solution states that for $\lambda_1 \neq 0$ and in the limit of large time, we recover asymptotically the usual Darcy model for Newtonian fluids with $\lambda_1 = \lambda_2 = 0$, namely, $\mathcal{H} - \Re \partial_x T = 0$.

The heat transfer rate is expressed in terms of the bulk-averaged Nusselt number defined as

$$Nu = -\left\langle \int_0^1 \partial_z T)_{z=0} dx \right\rangle, \tag{8}$$

where the angle brackets indicate the long-time average.

III. NUMERICAL METHOD AND VALIDATION

Systems (6a)-(6c) subjected to conditions (6d) and (6e) have been numerically solved using finite difference discretization with regular mesh.

Equation (6a) subjected to conditions (6d) is solved by the ADI method. To solve Equation (6b), the space derivative of temperature is approximated by a standard second-order centered scheme, and its temporal derivative is obtained by means of (6a). Using the already obtained temperature fields T^n and T^{n+1}, Equation (6b) becomes an ordinary temporal differential equation. We resolve it with a second order Runge-Kutta method. To find the stream function, we discretize Poisson equation (6c) by a standard centered second order scheme and resolve it by the successive over-relaxation (SOR) method. We use the Chebyshev acceleration in order to reduce the required total number of iterations. To clarify, a summary of the principal steps is given as follows:

1. Solve (6a) with updated ψ (i.e., u, w) and T or initial guess values $\psi^0 = 0, T^0 = 1 - z \forall (x, z)$.
2. Approximate $\partial_x T$ by a standard second-order centered scheme.
3. Approximate $\partial_t (\partial_x T) = \partial_x (\partial_t T)$ using a standard second-order centered scheme; $\partial_t T$ is obtained from (6a).
4. Calculate $\Re (1 + \lambda_2 \partial_t) \partial_x T$ from 2 to 3.
5. Solve (6b) which become an ODE, using a second order Runge-Kutta method.
6. Solve Poisson equation (6c) with SOR method, using Chebyshev acceleration.
7. Verify convergence criterion (quadratic norm of residual's sum $<10^{-12}$).
8. If criterion 7 is not satisfied, then return to step 1.
9. If criterion 7 is satisfied, then increment the time and return to step 1.

To verify the accuracy of our numerical simulation results, we perform two tests as follows:

1. The limiting case of a Newtonian fluid (see Table I).
2. The general case of a viscoelastic flow (see Table II).

TABLE I. Results from the present numerical scheme with $\lambda_1 = \lambda_2 = 0.001$ and from the work of Caltagirone[22] and Mahidjiba[23] in the Newtonian fluid case $\lambda_1 = \lambda_2 = 0$.

	$\Re = 100$			$\Re = 200$		
	This work	Caltagirone	Mahidjiba	This work	Caltagirone	Mahidjiba
Nu	2.6532	2.651	2.625	3.824	3.813	3.792
ψ_{max}	6.3501	5.377	5.354	8.9299	8.942	8.937
$N_x \times N_y$		32×32			48×48	

TABLE II. Comparison with Fu *el al.*[17] of critical Rayleigh numbers and critical frequencies.

(λ_1, λ_2)	$\Re_c$ Fu *et al.*	$\Re_c$ this work	Relative difference (%)	Frequency Fu *et al.*	Frequency this work	Relative difference (%)
(0.3, 0.2)	33.00	33.70	2.07	1.25	1.24	0.80
(0.2, 0.1)	29.70	30.45	2.46	2.40	2.39	0.41
(0.3, 0.1)	19.80	20.20	1.98	3.10	3.00	3.22

The results presented in the two tables show very good agreement with the literature data, either for the Newtonian flow or for the viscoelastic one. In Table I, we show the quantitative matching of the stream and heat transfer intensities, at two fixed values of the Rayleigh number. The computed results obtained for $\lambda_1 = \lambda_2 = 0.001$ converge asymptotically towards Newtonian fluids results with a relative difference of almost 1%.

In Table II, we compare our results with those given by Ref. 17 using three pairs of (λ_1, λ_2). We find that all the three cases present an oscillatory instability. We obtain the frequencies using Fourier transformation. A good agreement is observed. Furthermore, as we will see in Sec. IV, a perfect agreement is found between numerical and linear stability analysis results. Therefore, all these results suggest that our numerical algorithm can accurately simulate the problem of the present work.

IV. ONSET OF CONVECTION

The linear stability analysis is the starting point for treating the more realistic nonlinear problem. Since the latter is the main objective of the present work, we shall briefly sketch the linear analysis, by emphasizing the most important points and presenting new results for a domain of unit aspect ratio. The basic equations are obtained by linearizing sets (6a)–(6c) around the basic state

$$\psi_b = 0,\ T_b = 1 - z \tag{9}$$

and by seeking the two-dimensional perturbations $\psi, \theta = T - T_b$ verifying the boundary conditions of the form,

$$\psi = \psi_1 \sin(\pi z) \sin(m\pi x) \exp(\sigma t), \tag{10a}$$

$$\theta = \theta_1 \sin(\pi z) \cos(m\pi x) \exp(\sigma t), \tag{10b}$$

where m represents the number of convection rolls and $\sigma = \sigma_r + i\omega$ dictates the time evolution of the perturbation. The real part σ_r is the temporal growth rate, while ω represents the frequency of the oscillations. Substitution of (10a) and (10b) into the linearized version of (6a)–(6c) leads to the following results. There is a line of steady bifurcations given by $\Re_c^s = 4\pi^2$ for a single-cell convection which is the most unstable steady mode and a line of Hopf bifurcations along

$$\Re_c^{Osc}(m, \lambda_1, \lambda_2) = \frac{1 + m^2}{\lambda_1 m^2}(1 + \lambda_2 \pi^2 (1 + m^2)) \tag{11}$$

with the critical frequency

$$\omega_c(m) = \sqrt{\frac{1}{\lambda_2}[\pi^2(1 + m^2)(1 - \frac{\lambda_2}{\lambda_1}) - \frac{1}{\lambda_1}]} \tag{12}$$

provided $\lambda_1 > \lambda_1^\star = \lambda_2 + \frac{1}{\pi^2(1+m^2)}$ or equivalently $\lambda_2 < \lambda_2^\star = \lambda_1 - \frac{1}{\pi^2(1+m^2)}$.

As the critical Rayleigh number for the onset of oscillatory convection $\Re_c^{Osc}(m, \lambda_1, \lambda_2)$ depends on the number of rolls m, the relaxation time λ_1, and the retardation time λ_2, the true critical Rayleigh numbers may be ordered in a such way that

$$\Re_c^{Osc}(m, \lambda_1, \lambda_2) < \Re_c^{Osc}(m + 1, \lambda_1, \lambda_2) \tag{13}$$

for any integer m. According to expression (11), inequality (13) is satisfied only if

$$\lambda_2 > \frac{1}{\pi^2(m^2(1+m)^2-1)}. \tag{14}$$

In other words, the preferred mode of oscillatory instability is as follows:

(i) a mono-cellular flow (i.e., m = 1) if $\lambda_2 > \frac{1}{3\pi^2}$,
(ii) a two-cellular flow if $\frac{1}{35\pi^2} < \lambda_2 < \frac{1}{3\pi^2}$,
(iii) a three-cellular flow if $\frac{1}{143\pi^2} < \lambda_2 < \frac{1}{35\pi^2}$, and so on.

The Hopf curve branches off the steady bifurcation curve when

$$\Re = \Re^\star = \Re_c^{Osc} = 4\pi^2,\ \lambda_1 = \lambda_1^\star = \lambda_2 + \frac{1}{\pi^2(1+m^2)} \tag{15a}$$

or equivalently

$$\Re = \Re^\star = \Re_c^{Osc} = 4\pi^2,\ \lambda_2 = \lambda_2^\star = \lambda_1 - \frac{1}{\pi^2(1+m^2)}. \tag{15b}$$

At this point, the frequency of the oscillation is zero and we have a codimension-two double-zero bifurcation. In that point the linear theory fails to predict the dominant mode of convection. Therefore, a weakly nonlinear stability analysis is needed to elucidate the bifurcation processes near the codimension-two point $(\Re^\star, \lambda_1^\star)$.

The connection between linear theory and the numerically computed properties at the onset of convection is examined and presented in Fig. 2 for $\lambda_1 = 0.25; 0.5$, and 0.75. A close inspection of this figure demonstrates that a very good agreement is obtained between the linear stability theory (lines) and the numerical results (symbols). The critical Rayleigh number for the onset of oscillatory instability increases both with the increase of λ_2 for a fixed value of λ_1 or the decrease of λ_1 for a fixed value of λ_2, attesting the stabilizing effect of the retardation time and the destabilizing effect of the relaxation time. With regard to the question of the influence of the retardation time λ_2 on the pattern selection, Fig. 3 displays the onset of instability obtained numerically (symbols), as well as the true critical Rayleigh number curves $\Re_c^{Osc}(m)$ determined by linear theory (continuous line), as functions of λ_2 for $\lambda_1 = 0.75$. Also shown in this figure are the computed streamlines corresponding to the cases $\lambda_2 = 0.001$, $\lambda_2 = 0.01$, and $\lambda_2 = 0.035$, respectively. This figure shows that the true critical Rayleigh number $\Re_c^{Osc}(m)$ depends on λ_2. The numerically computed spatial patterns fall into the predictions of linear stability approach, namely, a three-cellular flow if $\frac{1}{143\pi^2} < \lambda_2 = 0.001 < \frac{1}{35\pi^2}$, a two-cellular flow if $\frac{1}{35\pi^2} < \lambda_2 = 0.01 < \frac{1}{3\pi^2}$, and a mono-cellular flow for $\lambda_2 = 0.035 > \frac{1}{3\pi^2}$.

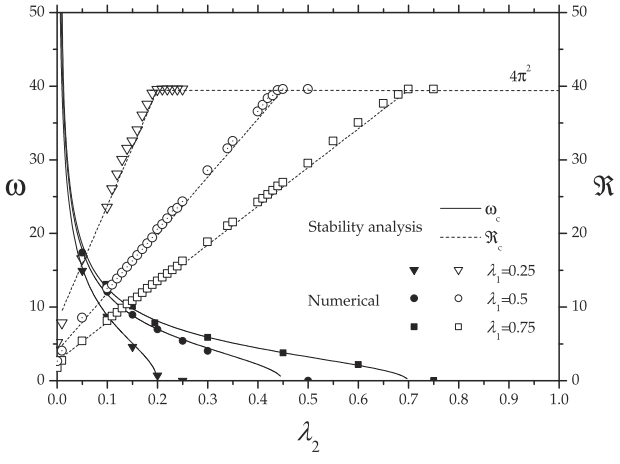

FIG. 2. Comparison between stability analysis and numerical results. Critical Rayleigh number and critical frequencies at the onset of convection as functions of the viscoelastic parameters.

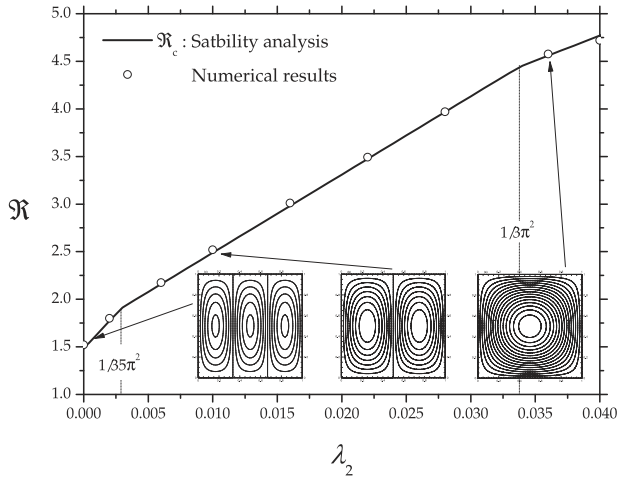

FIG. 3. Critical Rayleigh number versus retardation time with $\lambda_1 = 0.75$. Also shown are the streamlines for $\Re = 4.5$; $\lambda_2 = 0.035$ (a), $\Re = 2,5$; $\lambda_2 = 0.01$ (b), and $\Re = 1.7$; $\lambda_2 = 0.001$ (c).

V. RESULTS IN NONLINEAR REGIME

A. Normal form analysis

Once the onset of convective instability has been identified, an amplitude equation approach is used to determine the flow pattern bifurcations as functions of the control parameters $(\Re, \lambda_1, \lambda_2)$. In a recent paper, Hirata *et al.*[15] proposed a nonlinear reduced model by using perturbation techniques in the neighborhood of the codimension-two point $(\Re^\star, \lambda_1^\star)$. They derived the following system of nonlinear ordinary differential equations governing the dynamics of the normalized vertical velocity field W:

$$\begin{cases} \dfrac{dW}{dt} = Z(\mathrm{t}), & \text{(16a)} \\ \dfrac{dZ}{dt} = -W^3 + \mu_1 W + \mu_2 Z(\mathrm{t}) - W^2 Z(t), & \text{(16b)} \end{cases}$$

with $\mu_1 = \frac{f_2^2}{f_1^2}\frac{\Re - \Re_c^s}{2\lambda_2}$, $\mu_2 = \frac{f_2}{f_1}\frac{\lambda_1^\star(\Re - \Re_c^{Osc})}{2\lambda_2}$, $f_1 = \frac{1}{8\lambda_2}$, and $f_2 = -\frac{1}{\lambda_2}[\frac{5}{16\pi^2} - \frac{3\lambda_1^\star}{8} + \frac{3}{8\lambda_2}(\frac{1}{4\pi^4} - \frac{\lambda_1^\star}{2\pi^2})]$.

The stability types of fixed points and limit cycles, the bifurcation lines, and the phase portrait associated with system (16) were analyzed by Hirata *et al.*[15] by using dynamic systems theory. The reader is also referred to the paper by Holmes and Rand[24] and to Chapter 7 of Ref. 25 for further details. The current section is focused on the main nonlinear results with the objective to aid comparison between theoretical predictions and numerical results. For this purpose, we have first drawn the bifurcation set for the case $\lambda_1 = 0.5$ in $(\lambda_2, \Re)$ parameter plane, as shown in Fig. 4. We can see that the $(\lambda_2, \Re)$ plane is divided into six regions separated by five lines. In this figure, the line $\Re = \Re_c^{Osc}$ (i.e.,$\mu_2 = 0$) is the line of Hopf bifurcation points for which Eqs. (11) and (12) hold. The line $\Re_c^s = 4\pi^2$ (i.e., $\mu_1 = 0$) is the line of pitchfork bifurcation points. These two lines intersect at the codimension-two point$(\lambda_2^\star = \lambda_1 - \frac{1}{2\pi^2}, \Re^\star = 4\pi^2)$. The oscillatory convection induced by the Hopf bifurcation is the only stable pattern for $\Re < \Re_{NL1}$ (i.e., regions II and III in Fig. 4). The two types of convective patterns, namely, oscillatory and stationary convection coexist between the nonlinear thresholds $\Re_{NL1}$ (i.e., $\mu_2 = \mu_1$) and $\Re_{NL3}$ (i.e., $\mu_2 = 0.752\mu_1$). The observability of either oscillatory convection or stationary one depends on the initial conditions. The line $\Re = \Re_{NL2}$ (i.e., $\mu_2 = 4/5\mu_1$) corresponds to a double homoclinic bifurcation points. The appearance of such orbits is often the precursor to a transition to chaos.[26] Therefore one may expect a rich dynamics in the neighborhood of this line. The line $\Re = \Re_{NL3}$ represents the nonlinear threshold for the transition from oscillatory convection to stable stationary one independently of initial conditions. This means physically that the viscoelasticity of the fluid has no influence on the

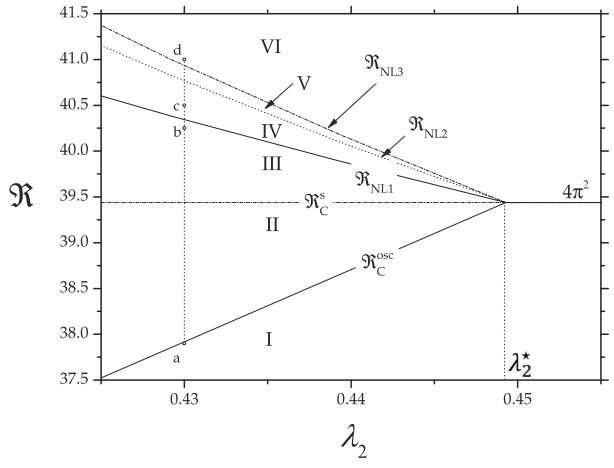

FIG. 4. Bifurcation lines according to weakly nonlinear theory for $\lambda_1 = 0.5$.

convection properties and the system behaves like a Newtonian fluid when the Rayleigh number slightly exceeds the nonlinear threshold $\Re_{NL3}$.

It is of great interest to investigate the effects of the viscoelastic parameters λ_1 and λ_2 on the nonlinear thresholds $\Re_{NL1}$, $\Re_{NL2}$, and $\Re_{NL3}$. Fortunately we succeeded in obtaining an explicit form of these nonlinear thresholds as a function of viscoelastic parameters. Let us define the following:

$$\Re_{NL}(\alpha) = 4\pi^2\left(1 + \frac{\omega_c^2\lambda_1\lambda_2^\star}{\alpha - 1 + 2\pi^2\lambda_2(3\alpha - 1)}\right). \tag{17}$$

Therefore we obtain

$$\Re_{NL1} = \Re_{NL}(\alpha = 1), \Re_{NL2} = \Re_{NL}(\alpha = 4/5), \text{ and } \Re_{NL3} = \Re_{NL}(\alpha = 0.752). \tag{18}$$

More importantly, the analytical expressions $\Re_{NL1}$ and $\Re_{NL3}$ can be used to determine the effect of the relaxation time λ_1 and the retardation time λ_2 on the nonlinear threshold for the possible transition from oscillatory to stable stationary convection. We found that both $\Re_{NL1}$ and $\Re_{NL3}$ decrease with an increasing λ_2 and increase with an increasing λ_1 as it is seen in Fig. 4 and in Fig. 6(a), respectively. In other words, when the relaxation time increases, more heating is needed for stationary convection to suppress oscillatory convection, whereas an opposite trend is observed when the retardation time is increased.

B. Numerical results

The present section is devoted to the discussion of the above theoretical predictions in relation to two-dimensional numerical simulations of the full problem.

Different numerical simulations will be performed, first for $\lambda_1 = 0.5$ and $\lambda_2 = 0.43$ at selected values of Rayleigh number $\Re$. The corresponding points in the $(\lambda_2, \Re)$ plane are in Fig. 4 and labeled from (a)–(d). The time history of the Nusselt number Nu is shown in Fig. 5 for the six selected cases. The results obtained in the different cases are now briefly described.

(1) Points (a) and (b): for these cases (Figs. 5(a) and 5(b), respectively), we see that for $\Re = 37.9 < \Re_c^{Osc} = 37.95$, Nu tends to 1 indicating that the heat transfer is due only to the conduction mechanism. For $\Re = 40.25$ above the linear critical threshold $\Re_c^{Osc}$, Nu oscillates in time with a well-defined Hopf frequency corresponding to the emergence of a limit cycle, as it is predicted by the normal form analysis.

(2) Point (c): for this case the value of Rayleigh number $\Re = 40.5$ is chosen between $\Re = \Re_{NL1}$ and $\Re = \Re_{NL3}$ given by analytical expressions (17) and (18). The conduction state and the oscillatory convection state obtained in the two previous runs, respectively, for $\Re = 37.9$

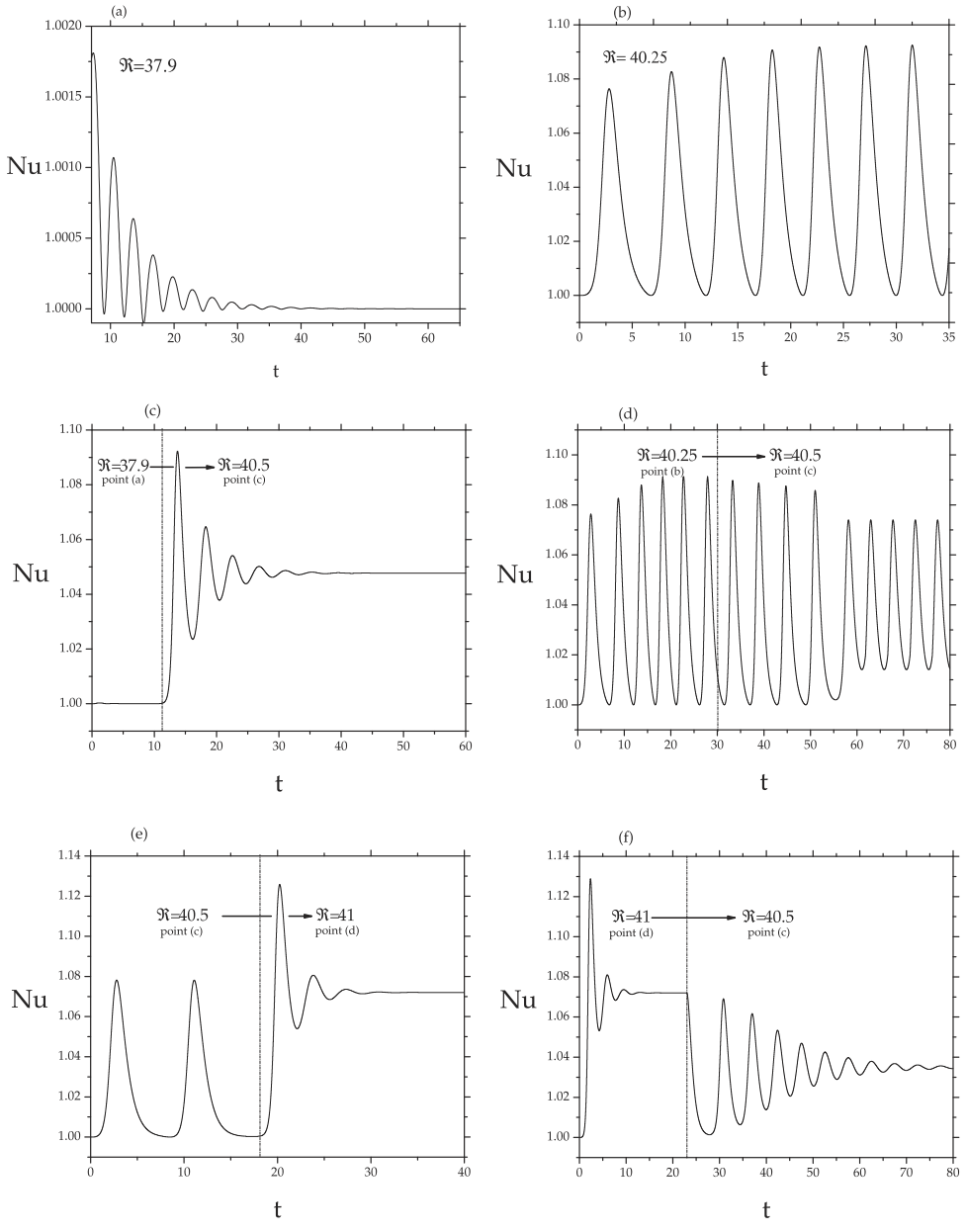

FIG. 5. Time history of Nusselt number for several representative values of Rayleigh number corresponding to points (a)-(d) of Fig. 4 with $\lambda_1 = 0.5$.

(point (a)) and for $\mathfrak{R} = 40.25$ (point (b)) are two different initial conditions used for the present runs. Figure 5(c) shows that the conduction state is maintained until $t = 11$, time at which the Rayleigh number is suddenly increased to $\mathfrak{R} = 40.5$ (point (c)). As we can observe, the *Nu* curve appears to be constant at large time attesting the steady nature of the convection. On the other hand, Fig. 5(d) shows that the final convective state is periodic in time if the point (c) is reached from the oscillatory state obtained in the point (b). These two runs confirm that for $\mathfrak{R}_{NL1} < R < \mathfrak{R}_{NL3}$, the solution depends on the initial conditions as predicted by the nonlinear stability analysis.

(3) Point (d): in this case oscillatory convective state obtained from the previous run with $\mathfrak{R} = 40.5$ (point (c)) is used as initial conditions for the computations performed here with increasing Rayleigh number to $\mathfrak{R} = 41$ at time $t = 18$. The result of this run is presented in Fig. 5(e),

showing that Nu curve appears to be constant at large time, which means that oscillatory convection is replaced by a stationary one.

(4) Back to the point (c): starting a run from the developed stationary convection obtained with $\mathfrak{R} = 41$ (point (d)), and decreasing $\mathfrak{R}$ to $\mathfrak{R} = 40.5$ (back to the point (c)), we do not recover oscillatory convection as it can be concluded from the stationary behavior of Nusselt number shown in Fig. 5(e). By ramping $\mathfrak{R}$ forth and back between points (c) and (d), the numerical results showed that the convection exhibits hysteresis in the second transition oscillatory/stationary convection.

In order to assess the validity of the theoretical results for different set of parameters, we computed the bifurcation line from oscillatory convective pattern to stationary one for either a fixed value of λ_2 with varying values of λ_1 or a fixed value of λ_1 with varying values of λ_2. For all cases examined in the following, the initial conditions used are a rest state on the entire domain, except on a random point where we set infinitesimal perturbation $\psi = 10^{-9}$. In Fig. 6(a), we compare theoretical results (bold continuous lines) corresponding to the nonlinear thresholds $\mathfrak{R}_{NL1}$ and $\mathfrak{R}_{NL3}$ of a possible transition from oscillatory to steady convection in the $(\lambda_1, \mathfrak{R})$ plane for $\lambda_2 = 0.2$

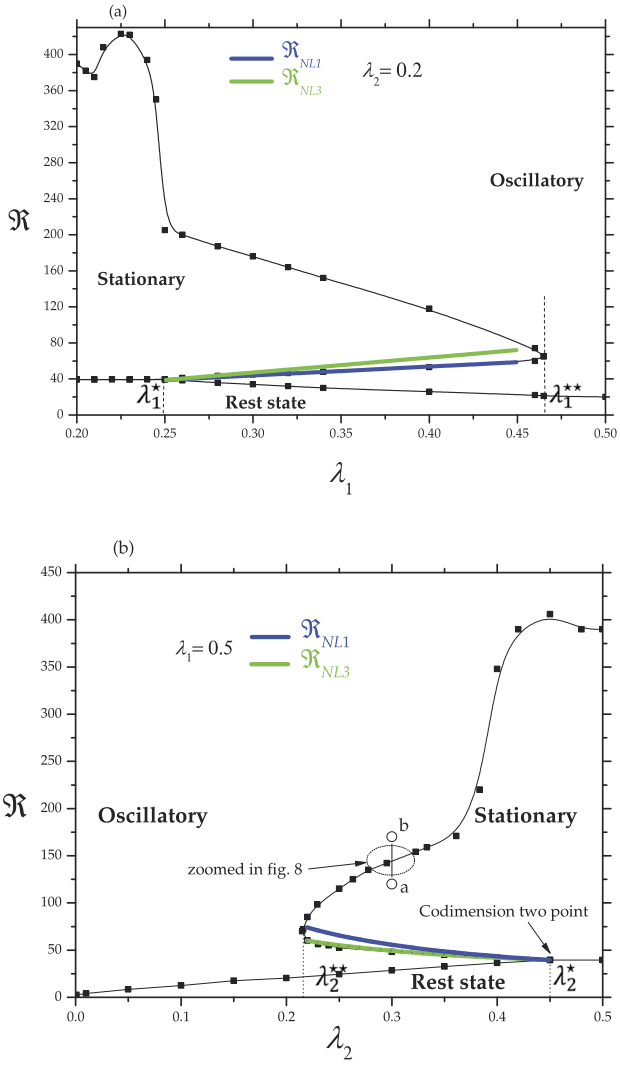

FIG. 6. General stability diagram for $\lambda_2 = 0.2$ in the $(\lambda_1, \mathfrak{R})$ plane (a) and for $\lambda_1 = 0.5$ in the $(\lambda_2, \mathfrak{R})$ plane (b). $\mathfrak{R}_{NL1}$ (the lower bold line) and $\mathfrak{R}_{NL3}$ (the upper bold line) correspond to the nonlinear thresholds derived from weakly nonlinear stability analysis.

TABLE III. Values of $\lambda_2^\star$ and $\lambda_2^{\star\star}$ for $\lambda_1 = 0.25$, 0.5, and 0.75.

	$\lambda_1 = 0.25$	$\lambda_1 = 0.5$	$\lambda_1 = 0.75$
$\lambda_2^{\star\star}$	0.107	0.215	0.345
$\lambda_2^\star$	0.200	0.450	0.697

with the results computed by direct two-dimensional simulations (solid square symbols). As can be seen from this figure, the theoretical line $\mathfrak{R}_{NL1}$ ($\mathfrak{R}_{NL3}$) merges into (is tangent to) the numerically computed curve. Nevertheless, the numerical results reveal that a transition to steady convection is observed only for $\lambda_1 < \lambda_1^{\star\star}$, i.e., for a relatively weak elastic fluid. Additional computations, not shown here, demonstrated that the maximal value $\lambda_1^{\star\star}$ depends on the retardation time λ_2. Changing λ_2 produced only quantitative differences in the results. This finding may explain why numerical experiments of Ref. 17 (see Fig. 1) conducted with $\lambda_2 = 0.1$ revealed the existence of a transition from oscillatory convection to stationary one for the case $\lambda_1 = 0.2$, while this transition never occurs for the case $\lambda_1 = 0.3$. In the same manner, the effect of the retardation time λ_2 on the secondary bifurcation to a steady convection state is illustrated in Fig. 6(b) for $\lambda_1 = 0.5$. In this figure the nonlinear theoretical thresholds $\mathfrak{R}_{NL1}$ and $\mathfrak{R}_{NL3}$ are represented by a bold continuous line, while squares are numerical results. As it is shown in Fig. 6(b), we observe a very good agreement between theory and numerical simulations in the neighbourhood of the codimension-two bifurcation point. Moreover, computed transition line to steady state convection attests the existence of a minimal value $\lambda_2^{\star\star}$ below which no such transition can occur. In other words, the transition from an oscillatory pattern to a steady one is only possible if $\lambda_2 \in]\,\lambda_2^{\star\star},\ \lambda_2^\star\,[$, where $\lambda_2^\star$ and $\lambda_2^{\star\star}$ depend on λ_1. In Table III, we give the computed values of $\lambda_2^\star$ and $\lambda_2^{\star\star}$ for $\lambda_1 = 0.25, 0.5,$ and 0.75.

Once again this result may explain why in the numerical simulations of Ref. 17 (see Fig. 1) with $\lambda_1 = 0.3$, oscillatory convection for the case $\lambda_2 = 0.2$ is completely suppressed and replaced by a stationary convection when $\mathfrak{R}$ reaches a critical value, contrary to the case $\lambda_2 = 0.1$ where independently of $\mathfrak{R}$ the system never experiences this transition.

Up to now there are already several interesting points deserving to be remarked.

1. Two-dimensional numerical simulations show that in the parameter space where the system exhibits a first Hopf bifurcation, a secondary transition may occur to a steady state. It is found that convection exhibits hysteresis near this transition. The threshold Rayleigh number for the onset of the secondary bifurcation is found to increase as a function of increasing the relaxation time λ_1 and to decrease with increasing the retardation time λ_2.
2. Guided by the results of the normal form analysis, we numerically determine the extension of the region where this transition is observed, as a function of the Rayleigh number and the viscoelastic parameters. It is found that the secondary bifurcation to a steady state may occur provided that either λ_1 do not exceed a particular value $\lambda_1^{\star\star}$ for a prescribed value of λ_2 or that λ_2 remains less than a particular value $\lambda_2^{\star\star}$ for a fixed value of λ_1. This finding gives a qualitative explanation of some numerical results of Ref. 17. Moreover, in the parameter space where this secondary transition is possible, it is found that the threshold Rayleigh number obtained numerically agrees very well with the nonlinear threshold determined analytically.

For reference purposes and according to the above finding, let us define three regions in the viscoelastic parameters plane: (i) a weakly viscoelastic regime refers to the region of viscoelastic parameters with $\lambda_1 < \lambda_1^\star$ or $\lambda_2 > \lambda_2^\star$ where the first instability has a steady character, (ii) a moderately viscoelastic regime corresponds to viscoelastic fluids with $\lambda_1^\star < \lambda_1 < \lambda_1^{\star\star}$ or $\lambda_2^{\star\star} < \lambda_2 < \lambda_1^\star$ where the system experiences a time periodic convection pattern as a first instability, followed by a secondary bifurcation to a steady mode of convection at a second critical value of the Rayleigh number, and (iii) a strongly viscoelastic regime refers to viscoelastic fluids with $\lambda_1 > \lambda_1^{\star\star}$ or $\lambda_2 < \lambda_2^{\star\star}$.

C. Computation of a secondary Hopf bifurcation far from the codimension-two point

In Sec. V B, the numerically computed dynamics associated with the nonlinear interaction between oscillatory and stationary instabilities was found to be in a good agreement with weakly nonlinear theory by using the time-dependent amplitude equation (16). In particular, the theoretical predictions were very useful in guiding the numerical experiments. However, it is important to emphasize that the derivation of the amplitude equation (16) is rigorously valid in the neighborhood of the codimension-two bifurcation point. For high values of Rayleigh number (i.e., $\Re \gg 4\pi^2$), the departure from the codimension-two point is very important implying that amplitude equation (16) ceases to be valid. Therefore only direct numerical simulations will be used in the following. One of our main points of interest centers on the question as to whether the primary and the secondary steady bifurcation observed, respectively, in the weakly and moderately viscoelastic regimes is stable against time-dependent disturbances. With regard to this question, it has been established that for a Newtonian fluid saturating a porous square box, a single-cell solution undergoes a series of bifurcations as the Rayleigh number is increased. At the second critical value of the Rayleigh number $\Re \approx 390$, a Hopf bifurcation has been observed for two-dimensional single-cell convection by, for instance, Schubert and Straus,[27] Kimura *et al.*,[28] and Aidun and Steen.[29]

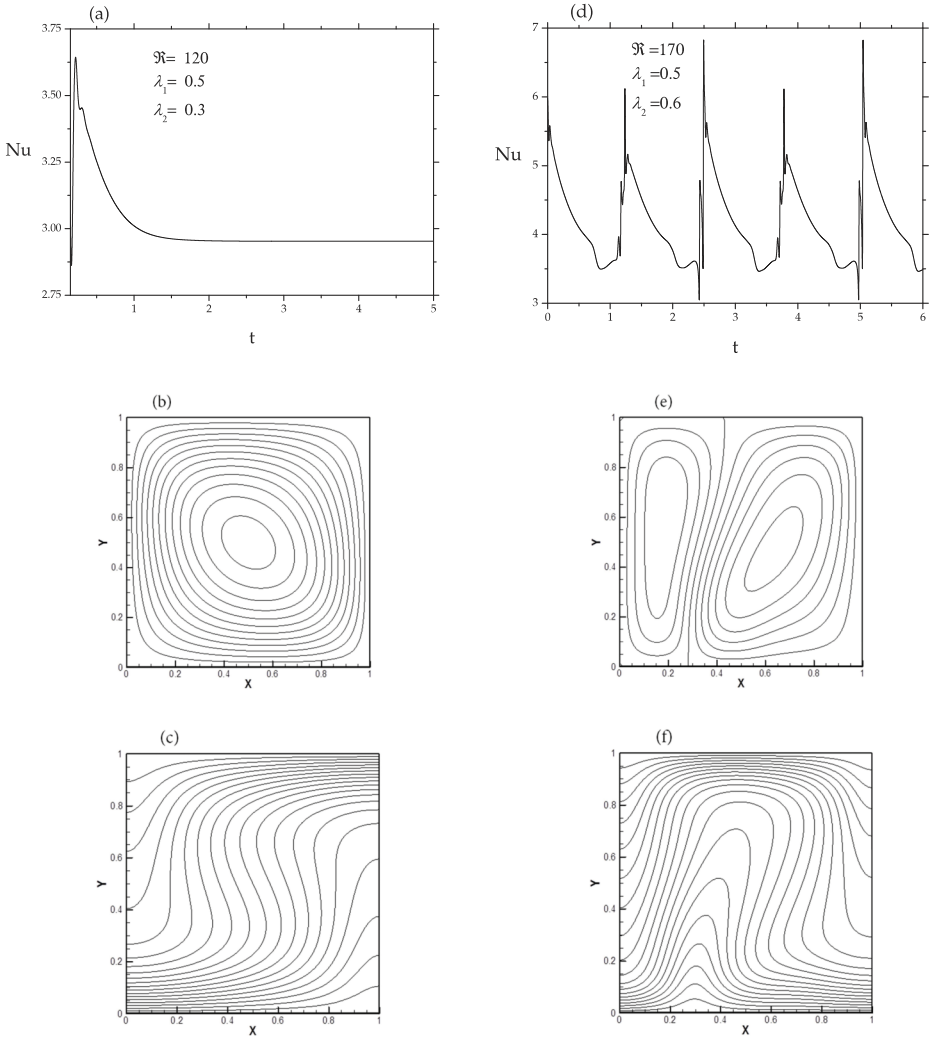

FIG. 7. Transition from stationary to oscillatory convection at high Rayleigh numbers. Are shown: Nusselt number versus time, streamlines, and temperature distribution for $\lambda_1 = 0.5$ and $\lambda_2 = 0.6$: $\Re = 120$ ((a)–(c)) and $\Re = 170$ ((d)–(f)).

The first set of results presented in this section involves fluids with the relaxation time $\lambda_1 = 0.5$ and the retardation time $\lambda_2 = 0.3$. Note that the prescribed value of λ_2 is chosen such that $\lambda_2 \in]\lambda_2^{\star\star} = 0.215, \lambda_2^{\star} = 0.45[$ (i.e., in moderately viscoelastic regime) in order to allow a secondary transition from oscillatory to steady convection flow. With the aim to locate a possible third transition, we computed the averaged Nusselt number Nu as a function of the Darcy-Rayleigh number $\mathfrak{R}$, starting our numerical experiments from the nonlinear threshold Rayleigh number corresponding to the transition to a steady convection state. By increasing $\mathfrak{R}$, we found that the steady state is the only stable state up to $\mathfrak{R} \approx 145$ where a second Hopf bifurcation develops. Shown in Figs. 7(a)-7(c) and 7(d)-7(f) the time dependence of Nu, the stream function and the temperature distribution before and after the observed third transition, namely, for $\mathfrak{R} = 120$ and $\mathfrak{R} = 170$, respectively. The corresponding points in the $(\lambda_2, \mathfrak{R})$ plane are in Fig. 6(b) and labeled (a) and (b), respectively. The averaged Nusselt number displayed in Fig. 7(a) appears to be constant at large time attesting the stationary character of the instability for $\mathfrak{R} = 120$. Moreover, as it is seen in Fig. 7(b) the fluid motion exhibits a single-cell convection. A further increase in Darcy-Rayleigh number to $\mathfrak{R} = 170$ changes drastically the temporal behavior as well as the spatial convection pattern. Indeed for $\mathfrak{R} = 170$ larger than the threshold where the secondary Hopf bifurcation may develop, the flow oscillates periodically, which results in the Nusselt number being oscillatory with time (Fig. 7(d)). Furthermore, the fluid motion exhibits a two-cellular flow as it is clearly shown by the snapshot of the corresponding stream function (Fig. 7(e)). In addition, comparison between the temperature distributions shown in Figs. 7(c) and 7(f) attests that the penetration of the thermal plume from the bottom thermal boundary layer is the physical origin for the observed emergence of a two-cellular flow instead of a single-cell convection.

Having analyzed the $\lambda_1 = 0.5$ and $\lambda_2 = 0.3$ case, it can now be used as a reference in the examination of the effects caused by both viscoelastic parameters on the Hopf bifurcation properties. In order to evaluate effect of the retardation time alone, varying values of λ_1 cases are numerically investigated with a fixed retardation time $\lambda_2 = 0.2$. On the other hand, the effect of the retardation time alone is studied by fixing $\lambda_1 = 0.5$ and varying λ_2. Here for the sake of brevity, we only focus on the results corresponding to the nonlinear threshold beyond which a new transition occurs giving rise to a Hopf bifurcation. The general bifurcation diagram is shown in $(\lambda_1, \mathfrak{R})$ plane for $\lambda_2 = 0.2$ (Fig. 6(a)), and in $(\lambda_2, \mathfrak{R})$ plane for $\lambda_1 = 0.5$ (Fig. 6(b)) where the upper curves correspond to the computed Hopf bifurcation lines up to $\mathfrak{R} = 420$. In order to have an overview summarizing in a single scheme all the main bifurcations, we also display in both figures the transition line to a first Hopf bifurcation determined by linear stability analysis (lower curves) and the transition line to a steady convection state (middle curves) determined previously. The two figures present a few interesting phenomena worth discussing in more detail. First among them concerns the successive bifurcations

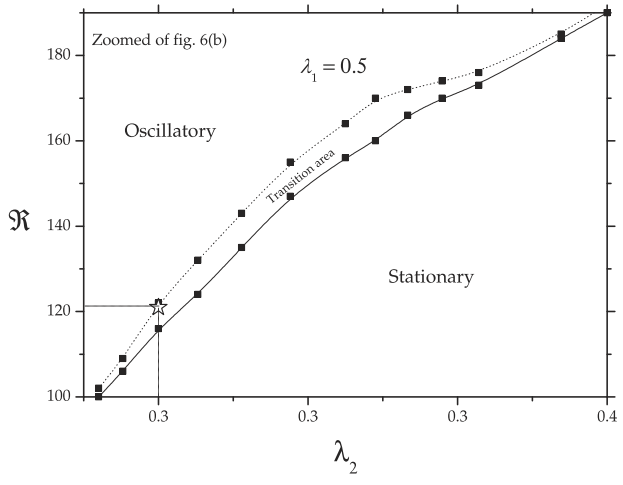

FIG. 8. Transition area from stationary to oscillatory convection (zoomed region of Fig. 6(b)).

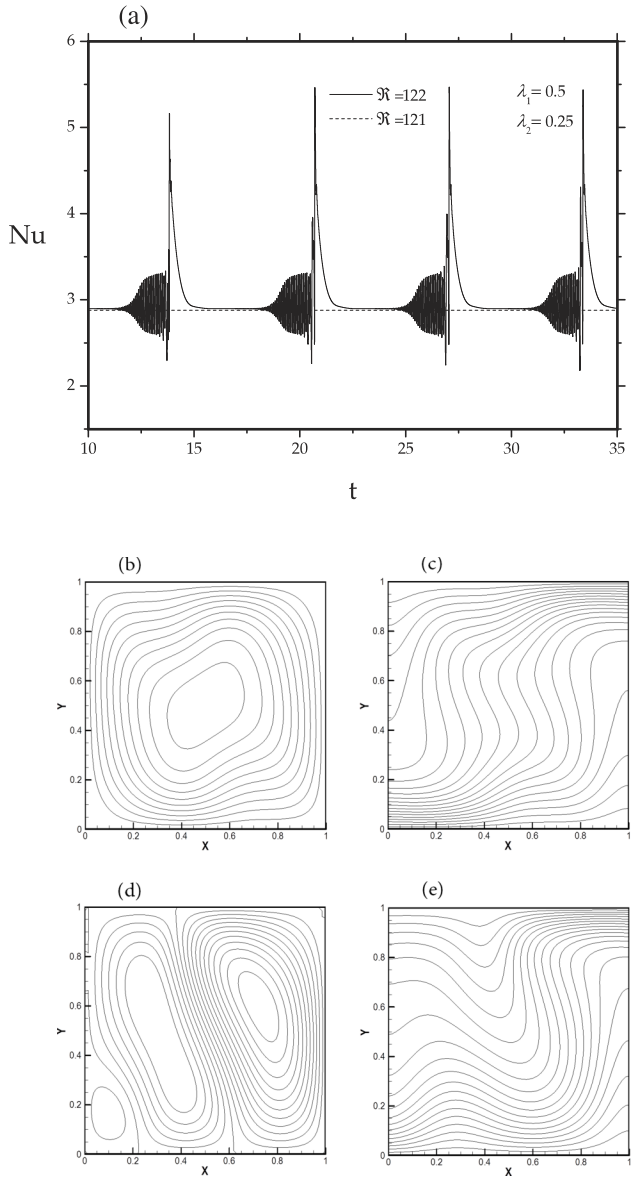

FIG. 9. Intermittent oscillation with steady state in the transition zone (star on Fig. 8): Nusselt variation at $\Re = 121$ and $\Re = 122$ (a) and corresponding snapshots of stream-function and isotherms at t = 17.5 ((b) and (c)) and t = 18.5 ((d) and (e)).

observed in the weakly elastic fluids (i.e., for $\lambda_1 < \lambda_1^\star = 0.25$ in Fig. 6(a) or $\lambda_2 > \lambda_2^\star = 0.45$ in Fig. 6(b). For these fluids, a first stationary bifurcation occurs at the well known critical Rayleigh number $\Re_c^s = 4\pi^2$. This means that the fluid elasticity has no effect on the first instability properties and the non-Newtonian fluid behaves as a Newtonian fluid. By increasing $\Re$ to a second critical value $\Re_2^{Osc}$, a Hopf bifurcation occurs and the steady convective pattern is replaced by oscillatory convection. A close inspection of Figs. 6(a) and 6(b) shows that the second critical Rayleigh number $\Re_2^{Osc}$ reaches its maximum for $\lambda_1 = \lambda_1^\star = 0.25$ and $\lambda_2 = \lambda_2^\star = 0.45$, respectively. When λ_1 is decreased from $\lambda_1^\star$ to $\lambda_1 = \lambda_2 = 0.2$ (see Fig. 6(a)) or λ_2 is increased from $\lambda_2^\star$ to $\lambda_2 = \lambda_1 = 0.5$ (see Fig. 6(b), $\Re_2^{Osc}$ decreases from its maximum and eventually joins the limit $\Re_2^{Osc} = 390$, corresponding to Newtonian fluids (Refs. 27–29). We conclude that the effect of the relaxation (retardation) time on the second transition to oscillatory convection is stabilizing (destabilizing) for weakly viscoelastic fluids.

Second, in moderately viscoelastic regime where the viscoelastic parameters are such that $\lambda_1 \in]\lambda_1^\star, \lambda_1^{\star\star}[$ or $\lambda_2 \in]\lambda_2^{\star\star}, \lambda_2^\star[$, three sources of instability act in a concert to select the dominant mode of instability, namely, the heating from below, the relaxation time, and the retardation time. The resulting dynamics in this regime may be understood for example by increasing Darcy-Rayleigh number for fixed values of viscoelastic parameters. The first convective instability is oscillatory rather than steady when Darcy-Rayleigh number exceeds the onset of the first Hopf bifurcation $\mathfrak{R}_c^{Osc}$ (region between the lower line and the middle line in Figs. 6(a) and 6(b)). It should be noted that this oscillatory convection is completely due to the viscoelastic character of the fluid. Our previous analytical and numerical investigations showed that more heating is needed to suppress the oscillatory instability. By increasing $\mathfrak{R}$ to a defined critical value, a secondary bifurcation occurs where a stationary pattern becomes the dominant mode of instability (region between the middle line and the upper line in Figs. 6(a) and 6(b)). Physically, this transition may be understood by the dominant viscous effect compared to the elastic contribution. Finally, at a third critical Rayleigh number $\mathfrak{R}_3^{Osc}$, a transition is observed as a secondary Hopf bifurcation giving rise to a new mode of oscillatory convection (region beyond the upper lines in Figs. 6(a) and 6(b)). It is interesting to note that the critical Rayleigh number $\mathfrak{R}_3^{Osc}$ observes a sharp decrease (i.e., a strongly destabilizing effect) when λ_1 exceeds the value $\lambda_1^\star$ by small amount or λ_2 is just below the value $\lambda_2^{\star\star}$.

A final remark should also be made. It is instructive to identify the dynamics near the third transition line from stationary convection to oscillatory mode of instability. Fig. 8 represents zoomed data corresponding to the dashed circle of Fig. 6(b). As indicated in Fig. 8 a transition area exists before the appearance of a secondary oscillatory mode of convection. For an illustration purpose, a discussion of the $\lambda_1 = 0.5$ and $\lambda_2 = 0.25$ case is provided for $\mathfrak{R} = 121$ and $\mathfrak{R} = 122$ (point identified by a star in Fig. 8). Fig. 9(a) displays the time history of the average-Nusselt number. It shows a stationary behavior of *Nu* for $\mathfrak{R} = 121$ while *Nu* experiences an intermittent evolution between a steady state and an amplified oscillatory state for $\mathfrak{R} = 122$. Moreover, as can be seen from Figs. 9(b) and 9(c), the steady state is a single cell pattern while the intermittent oscillatory state is a pattern composed by three cells flow. The Nusselt peaks correspond to the transition from a multi-cellular flow to a mono-cellular mode of convection.

Finally, it should be noted here that a different scenario occurs for a strongly elastic fluid (i.e., for $\lambda_1 > \lambda_1^{\star\star}$ or $\lambda_2 < \lambda_2^{\star\star}$). In this regime, the first observed destabilization is due mainly to the fluid elasticity which is therefore responsible for the appearance of an elastic-induced mode of instability in the form of oscillatory convection. Some preliminary computations conducted with high Rayleigh number showed that the nonlinear dynamics is quite complicated. The study of different bifurcations leading to a chaotic convective pattern is out of the scope of this paper.

VI. CONCLUSION

In the present paper, numerical and theoretical investigations were performed to assess the effect of the viscoelastic character of the fluid on bifurcations of thermal convection in a porous square cavity heated from below. The modified Darcy law based on the Oldroyd-B model was used for modeling the momentum equation. The dimensionless governing equations of the problem are solved by the finite difference method. The horizontal walls are assumed to be impermeable and perfectly conducting, while the vertical walls are considered adiabatic. In addition to Darcy-Rayleigh number $\mathfrak{R}$, two viscoelastic parameters play a key role when characterizing the spatio-temporal behavior of the instability, namely, the relaxation time λ_1 and the retardation time λ_2. The main results that have been obtained can be summarized as follows:

(i) Linear stability analysis and two-dimensional numerical simulations showed that oscillatory rolls are the most unstable ones if λ_1 exceeds a particular value $\lambda_1^\star(\lambda_2)$ or λ_2 is less than a certain value $\lambda_2^\star(\lambda_1)$. Otherwise, the stationary rolls are the most amplified mode of convection as in the case for Newtonian fluids. Moreover, the number of rolls when a first Hopf bifurcation occurs has been determined by linear theory as a function of λ_2 and is found to agree with two-dimensional numerical simulations.

(ii) The critical Rayleigh numbers for oscillatory and stationary instabilities coincide for $\lambda_1 = \lambda_1^\star$ or $\lambda_2 = \lambda_2^\star$ and therefore a codimension-two bifurcation occurs. A weakly nonlinear stability analysis is therefore used to describe the dynamics which result from the two competing instabilities in the neighborhood of the codimension-two bifurcation point. In particular, we give a simple analytical expression of the nonlinear threshold above which a second hysteretic bifurcation from oscillatory to stationary convective pattern is observed.

(iii) A series of suitable numerical experiments are conducted with Rayleigh number up to $\mathfrak{R} = 420$ and varying viscoelastic parameters. For weakly elastic fluids with $\lambda_1 < \lambda_1^\star$ or $\lambda_2 > \lambda_2^\star$, we determined a second critical value $\mathfrak{R}_2^{Osc}(\lambda_1, \lambda_2)$ above which the system exhibits a Hopf bifurcation from steady convective pattern to oscillatory convection. The well known limit of $\mathfrak{R}_2^{Osc}(\lambda_1 = 0, \lambda_2 = 0) = 390$ for Newtonian fluids is recovered and the fluid elasticity effect is found to delay the onset of the Hopf bifurcation (i.e., $\mathfrak{R}_2^{Osc}(\lambda_1, \lambda_2) > 390$ for weakly elastic fluids).

For sufficiently elastic fluids with $\lambda_1 > \lambda_1^\star$ or $\lambda_2 < \lambda_2^\star$, numerical simulations revealed that a secondary bifurcation from oscillatory to a steady state may occur provided that either λ_1 does not exceed a particular value $\lambda_1^{\star\star}$ for a prescribed value of λ_2 or λ_2 remains less than a particular value $\lambda_2^{\star\star}$ for a fixed value of λ_1. In this moderately elastic regime, in addition to the heating, both the elastic and viscous characters of the fluid act together in the destabilisation phenomena. In the parameter space where this secondary transition is possible, it is found that near the codimension-two bifurcation point, the threshold Rayleigh number $\mathfrak{R}_2^{st}$ obtained numerically agrees quite remarkably with the nonlinear threshold determined analytically. Moreover, for higher Rayleigh number, the system may experience a third transition to a second Hopf bifurcation at $\mathfrak{R} = \mathfrak{R}_3^{osc}(\lambda_1, \lambda_2)$, where the steady state convection is replaced by a new oscillatory mode of convection. In contrast to weakly elastic regime, this observed Hopf bifurcation occurs earlier than for Newtonian fluids (i.e., $\mathfrak{R}_3^{osc}(\lambda_1, \lambda_2) < 390$ for moderately elastic fluids). Additionally, we also note that in the vicinity of the second Hof bifurcation line, the system experiences an intermittent evolution between a steady state and an amplified oscillatory state.

Finally it should be noted here that the extension of the present work to study the influence of viscoelasticity on the bifurcation sequence leading to a chaotic convective pattern for higher Rayleigh number is postponed to a future investigation.

NOMENCLATURE

The units correspond to the dimensional variables with a *d* as exponent.

C	Heat capacity [J/K]
g	Gravity acceleration $[\mathrm{m/s^2}]$
H, H^d	Side of the square box [m]
K	Permeability $[\mathrm{m^2}]$
P^d	Pressure [Pa]
$\mathfrak{R}$	Rayleigh Darcy number $\mathfrak{R} = Ra \times \mathrm{Da}$
T, T^d	Temperature [K]
u, w, u^d, w^d	The velocity components [m/s]
x, z	Coordinate system

Greek symbols

β	Volumetric expansion $[\mathrm{K^{-1}}]$
γ	Deformation tensor
κ	Effective thermal diffusivity $[\mathrm{m^2 s^{-1}}]$
ρ	Density $[\mathrm{kg/m^3}]$
$\lambda_i; \lambda_i^d$	Relaxation ($i = 1$) and retardation ($i = 2$) times [s]
μ	Dynamic viscosity [Pa s]
ν	Kinematic viscosity $[\mathrm{m^2 s^{-1}}]$

σ	Heat capacity ratio between solid and liquid phases
τ	Stress tensor [Pa]
ψ	Stream function

Subscripts

$\boxdot_c$	Critical
$\boxdot_f$	Filtration
$\boxdot_{NL}$	Nonlinear
$\boxdot_0$	Reference state

Exponents

$\boxdot^n$	n$^{\text{th}}$ time step
$\boxdot^{Osc}$	Oscillatory
$\boxdot^{St}$	Stationary
$\boxdot^d$	Dimensional variable
$\boxdot^\star$	Codimension two
$\boxdot^{\star\star}$	Limit of moderately elastic zone

[1] M. Zhang, I. Lashgari, T. A. Zaki, and L. Brandt, "Linear stability analysis of channel flow of viscoelastic Oldroyd-B and FENE-P fluids," J. Fluid Mech. **737**, 249–279 (2013).
[2] T. Green III, "Oscillating convection in an elasticoviscous liquid," Phys. Fluids **11**, 1410–1413 (1968).
[3] C. M. Vest and V. S. Arpaci, "Overstability of a viscoelastic fluid layer heated from below," J. Fluid Mech. **36**, 613–623 (1969).
[4] M. Sokolov and R. I. Tanner, "Convective stability of a general viscoelastic fluid heated from below," Phys. Fluids **15**, 534–539 (1972).
[5] S. Rosenblat, "Thermal convection in a viscoelastic liquid," J. Non-Newtonian Fluid Mech. **21**, 201–223 (1986).
[6] H. M. Park and H. S. Lee, "Hopf bifurcations of viscoelastic fluids heated from below," J. Non-Newtonian Fluid Mech. **66**, 1–34 (1996).
[7] P. Kolodner, "Oscillatory convection in viscoelastic DNA suspensions," J. Non-Newtonian Fluid Mech. **75**, 167–192 (1998).
[8] J. Martinez-Mardones, R. Tiemann, and D. Walgraef, "Thermal convection thresholds in viscoelastic solutions," J. Non-Newtonian Fluid Mech. **93**, 1–15 (2000).
[9] Z. Li and R. E. Khayat, "Finite-amplitude Rayleigh-Bénard convection and pattern selection for viscoelastic fluids," J. Fluid Mech. **529**, 221–251 (2005).
[10] S. C. Hirata, L. S. de B.Alves, N. Delenda, and M. N. Ouarzazi, "Convective and absolute instabilities in Rayleigh-Bénard-Poiseuille mixed convection for viscoelastic fluids," J. Fluid Mech. **765**, 167–210 (2015).
[11] M. C. Kim, S. B. Lee, S. Kim, and B. J. Chung, "Thermal instability of viscoelastic fluids in porous media," Int. J. Heat Mass Transfer **46**, 5065–5072 (2003).
[12] D. Y. Yoon, M. C. Kim, and C. K. Choi, "The onset of oscillatory convection in a horizontal porous layer saturated with viscoelastic liquid," Transp. Porous Media **55**, 275–284 (2004).
[13] S. C. Hirata and M. N. Ouarzazi, "Three-dimensional absolute and convective instabilities in mixed convection of a viscoelastic fluid through a porous medium," Phys. Lett. A **374**, 2661–2666 (2010).
[14] Z. Zhang, C. I. Fu, and W. Tan, "Linear and nonlinear stability analyses of thermal convection for Oldroyd-B fluids in porous media heated from below," Phys. Fluids **20**, 084103 (2008).
[15] S. C. Hirata, G. Ella Eny, and M. N. Ouarzazi, "Nonlinear pattern selection and heat transfer in thermal convection of a viscoelastic fluid saturating a porous medium," Int. J. Therm. Sci. **95**, 136–146 (2015).
[16] N. Delenda, S. Hirata, and M. N. Ouarzazi, "Primary and secondary instabilities of viscoelastic mixtures saturating a porous medium: Application to separation of species," J. Non-Newtonian Fluid Mech. **181**, 11–21 (2012).
[17] C. J. Fu, Z. Y. Zhang, and W. C. Tan, "Numerical simulation of thermal convection of a viscoelastic fluid in a porous square box heated from below," Phys. Fluids **19**, 104107 (2007).
[18] J. Niu, C. Fu, and W. Tan, "Thermal convection of a viscoelastic fluid in an open-top porous layer heated from below," J. Non-Newtonian Fluid Mech. **165**, 203–211 (2010).
[19] J. Niu, Z. Shi, and W. C. Tan, "The viscoelastic effects on thermal convection of an Oldroyd-B fluid in open-top porous media," J. Hydrodyn. **25**, 639–642 (2013).
[20] J. Niu, Z. Shi, and W. C. Tan, "Numerical simulation of thermal convection of viscoelastic fluids in an open-top porous medium with constant heat flux," J. Hydrodyn. **27**, 52–61 (2015).
[21] M. G. Alishayev and A. K. Mirzadjanzade, "For the calculation of delay phenomenon in filtration theory," Izvestya Vuzov, Neft Gaz. **6**, 71–77 (1975).
[22] J. P. Caltagirone, "Thermoconvective instabilities in a horizontal porous layer," J. Fluid Mech. **72**, 269–287 (1975).
[23] A. Mahidjiba, "Convection naturelle thermosolutale au sein d'une couche poreuse horizontale," M.S. thèsis, École Polytechnique de Montréal, 1998.
[24] P. Holmes and D. Rand, "Phase portraits and bifurcations of the non-linear oscillator: $x'' + (\alpha + \gamma x^2)\, x' + \beta x + \delta x^3 = 0$," Int. J. Non-Linear Mech. **15**, 449–458 (1980).

[25] J. Guckenheimer and P. Holmes, *Nonlinear Oscillations, Dynamical Systems, A Bifurcation of Vector Fields* (Springer-Verlag, New York, 1983).
[26] M. N. Ouarzazi, P. A. Bois, and M. Taki, "Nonlinear interaction of convective instabilities and temporal chaos of a fluid mixture in a porous medium," Eur. J. Mech., B: Fluids **13**, 423–438 (1994).
[27] G. Schubert and J. M. Straus, "Transitions in time-dependent thermal convection in fluid-saturated porous media," J. Fluid Mech. **121**, 301–313 (1982).
[28] S. Kimura, G. Schubert, and J. M. Straus, "Route to chaos in porous-medium thermal convection," J. Fluid Mech. **166**, 305–324 (1986).
[29] C. K. Aidun and P. H. Steen, "Transition to oscillatory convective heat transfer in a fluid saturated porous medium," J. Thermophys. Heat Transfer **1**, 268–273 (1987).